Conformational Cycling within the Closed State of Grp94, an Hsp90-Family Chaperone

Bin Huang, Larry J. Friedman, Ming Sun, Jeff Gelles and Timothy O. Street

Department of Biochemistry, *Brandeis University, Waltham, MA 02454, USA*

Correspondence to Timothy O. Street: *tstreet@brandeis.edu.*
https://doi.org/10.1016/j.jmb.2019.06.004

Abstract

The Hsp90 family of chaperones requires ATP-driven cycling to perform their function. The presence of two bound ATP molecules is known to favor a closed conformation of the Hsp90 dimer. However, the structural and mechanistic consequences of subsequent ATP hydrolysis are poorly understood. Using single-molecule FRET, we discover novel dynamic behavior in the closed state of Grp94, the Hsp90 family member resident in the endoplasmic reticulum. Under ATP turnover conditions, Grp94 populates two distinct closed states, a relatively static ATP/ATP closed state that adopts one conformation, and a dynamic ATP/ADP closed state that can adopt two conformations. We constructed a Grp94 heterodimer with one arm that is catalytically dead, to extend the lifetime of the ATP/ADP state by preventing hydrolysis of the second ATP. This construct shows prolonged periods of cycling between two closed conformations. Our results enable a quantitative description of how ATP hydrolysis influences Grp94, where sequential ATP hydrolysis steps allow Grp94 to transition between closed states with different dynamic and structural properties. This stepwise transitioning of Grp94's dynamic properties may provide a mechanism to propagate structural changes to a bound client protein.

Introduction

The Hsp90 family of molecular chaperones facilitates the folding and maintain the stability of their "client" proteins. Metazoans express four Hsp90 paralogs: Hsp90α and Hsp90β in the cytosol, Trap-1 in mitochondria, and Grp94 in the endoplasmic reticulum. All Hsp90s share a conserved domain organization [N-terminal domain, middle domain (MD), C-terminal domain (CTD)], and each paralog requires ATP binding and hydrolysis to chaperone their respective client proteins [1–3]. ATP binding stabilizes a closed, hydrolytically active, chaperone conformation. Two types of closed conformations have been observed. The p23-stabilized closed state of yeast Hsp90 (Hsp82) [4], the kinase-bound closed state of human Hsp90 [5], and the AMPPNP stabilized closed state of Grp94 [6] all have a symmetric closed conformation. In contrast, the closed state of Trap-1 has an asymmetric conformation in which the MD/CTD orientation on one arm is different from the other arm. This asymmetric state can be differentiated from a symmetric closed conformation via small-angle x-ray scattering (SAXS) measurements [7].

Despite advances in structural information for various Hsp90 conformations, it is not known how the cycle of ATP binding and hydrolysis by Hsp90 affects client protein folding. Particularly important is that all the above closed structures of Hsp90 are stabilized by two bound ATP molecules. As a result, many questions remain about what happens to the structure of the closed state upon ATP hydrolysis. Hsp90 remains biologically functional when the N-terminal domains are locked together via the addition of a coiled-coil sequence [8], which raises the possibility that ATP-dependent conformational changes within the Hsp90 closed state could provide its essential chaperoning function.

Because the conformation of Hsp90 changes dramatically between the open and closed states, FRET is a powerful tool for studying conformational kinetics and its regulation. However, bulk FRET measurements of yeast, bacterial, and mitochondrial

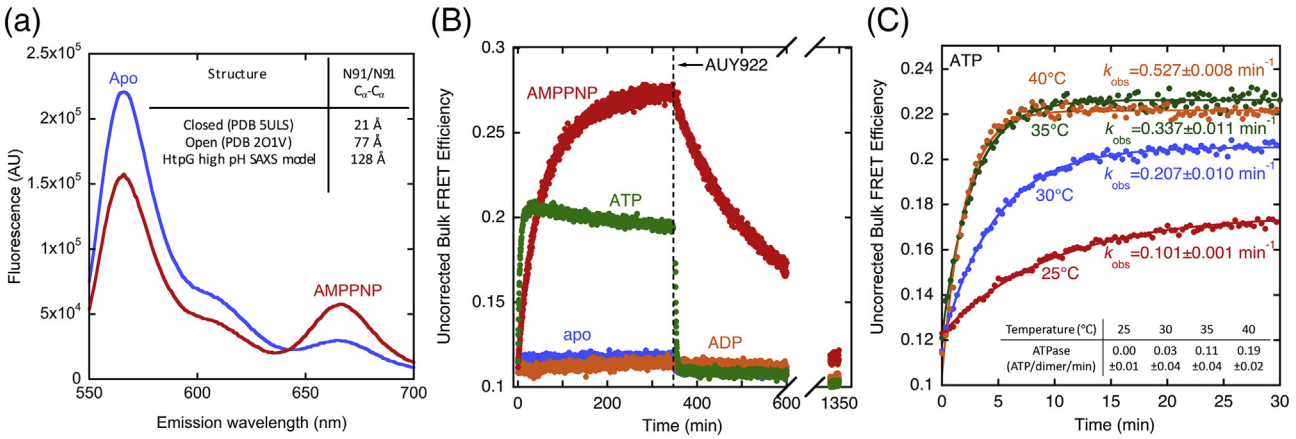

Fig. 1. Bulk FRET measurements of Grp94 with various nucleotides. (A) The N91/N91 FRET pair shows anti-correlated changes in bulk fluorescence spectra between apo and AMPPNP conditions. The activity of the labeled protein at 40 °C (0.22 ± 0.01 ATP/min/dimer) is similar to the wild-type rate (0.19 ± 0.02 ATP/min/dimer). Inset shows expected distances between the donor and acceptor in the open and closed states (PDB IDs: 2O1V, 5ULS). (B) The N91/N91 FRET pair shows an intermediate population of the Grp94 closed state with ATP at 30 °C. Grp94 reopens upon the addition of 500 μM AUY922. (C) Temperature-dependent closed-state accumulation with ATP. Solid lines are single exponential fits. Error bars on closure rates and activity values are the SEM. Buffer conditions: 25 mM Hepes (pH 8.0), 150 mM KCl, 600 μM $MgCl_2$, 600 μM nucleotides, 0.5 mg/ml BSA, 2 mM BME.

Hsp90 homologs, all show minimal population of the closed state under ATP turnover conditions [9–12]. Due to the lack of a well-populated closed state under ATP turnover conditions, closure kinetics in bulk have been measured with weakly hydrolyzing ATP analogs (AMPPNP and ATPγS). Hsp90 closure rates measured with these analogs are typically 10-fold slower than ATP hydrolysis rates [9,11,13], indicating that they are imperfect mimics of ATP. As a consequence, the transient nature of the closed state under ATP turnover conditions has imposed a practical challenge in constructing quantitative models describing the ATP-driven conformational cycle of Hsp90. The transient closed state has also made it difficult to study what happens to the closed state of Hsp90 when ATP is hydrolyzed. In particular, the role of the mixed ATP/ADP state, which must exist in the cycle, remains poorly understood and is an active area of research [10,12,14].

FRET measurements of Grp94 show closure with AMPPNP [6]; however, the magnitude of the FRET change is expected to be small with the previously used FRET pair based on the Grp94 open and closed crystal structures. We initially sought to design and test a new FRET pair for Grp94. However, in doing so, we discovered that Grp94 has a highly populated closed state under ATP turnover conditions. This characteristic reveals two modes of dynamic behavior in the Grp94 closed state.

Results

We used computational analysis to exhaustively evaluate possible fluorophore labeling sites to identify a solvent-exposed FRET pair that predicts a large distance change between the Grp94 open to closed crystal structures. Residue N91, which has an inter-arm C_α to C_α distance of 77 Å in the open state and 21 Å in the closed state, was selected for labeling. Labeling Grp94 at these sites yields ATPase activity essentially identical to wild-type, and AMPPMP-induced closure produces a large FRET increase (Fig. 1A). As a comparison, we tested the FRET pair used previously with Grp94 (labeling at E131/Q453 on opposite arms). Consistent with previous measurements [6], a small increase in FRET is observed upon closure (Supplemental Fig. 1A). The small change of FRET observed with the E131/Q453 pair suggests that the open-state conformation of Grp94 under our conditions is better described by the open-state crystal structure of Grp94 *versus* the fully open conformation observed for HtpG at high pH (see FRET pair distances in Supplemental Fig. 1A). The N91/N91 pair and E131/Q453 pair have comparable closure rates with AMPPNP, but the N91/N91 pair has a much greater magnitude of FRET change (Supplemental Fig. 1B). We next focused on exploring the N91/N91 FRET pair in detail.

The Grp94 closed conformation is well populated under ATP conditions

Figure 1B shows a representative closure and reopening experiment under AMPPNP and ATP conditions. Closure is 10-fold faster with ATP than with AMPPNP, but only reaches an intermediate level of FRET compared to AMPPNP. After ATP-driven closure has reached a steady state, reopening is initiated by addition of a tight binding ATP-competitive inhibitor (AUY922). For the ATP sample, reopening occurs quickly, whereas for AMPPNP, this process is slow. As expected, analogous experiments under apo and ADP conditions show no change of FRET. Grp94 closure rates and the closed-state population both increase with increasing temperature (Fig. 1C). As expected for a build-up of the closed conformation, closure is faster than steady-state ATP hydrolysis.

Grp94 changes conformation prior to opening

The highly populated closed state of Grp94 under ATP turnover conditions suggests that single-molecule FRET (smFRET) could reveal conformational intermediates that are sampled upon ATP hydrolysis but hidden in the bulk measurements. A biotinylated Grp94 construct was tethered at low density to a PEG/PEG-biotin derivatized microscope slide coated with streptavidin (Methods). Grp94 samples were pre-incubated with nucleotide to achieve an equilibrium condition for ADP or AMPPNP or steady-state condition for ATP. Illustrative microscope field images of donor and acceptor emission are shown in Supplemental Fig. 2.

Individual molecules of Grp94 exist in stable, well-separated open and closed conformation FRET states under ADP and AMPPNP conditions (Fig. 2). The closed state has significantly higher FRET efficiency than was seen in bulk (Fig. 1B); this is expected because the bulk data include dimers with donor but no acceptor, whereas the single-molecule analysis includes only dimers labeled with both donor and acceptor. Under ATP conditions (Fig. 2; Supplemental Fig. 3A–F), individual molecules of Grp94 are seen to transition between a high FRET state that is similar to AMPPNP and a low FRET state that similar to ADP. A high level of reproducibility for FRET efficiency profiles is observed for measurements taken at different fields of view on the same slide and for measurements taken on a different day with a different slide (Supplemental Fig. 3G–I).

An additional, higher FRET state is visually evident immediately prior to opening transitions. Figure 3A shows an example in which this higher FRET state has an extended lifetime. We identified all traces with

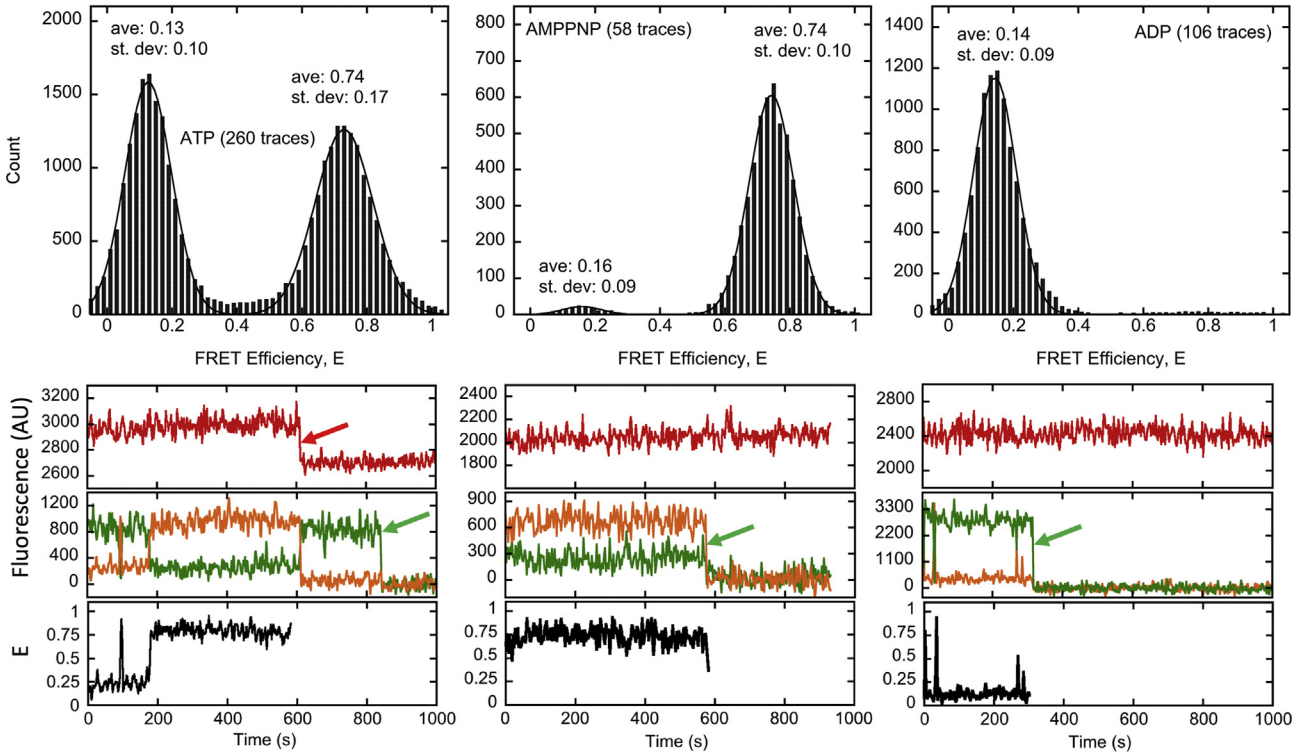

Fig. 2. smFRET measurements of Grp94 with various nucleotides. FRET of individual Grp94 dimers labeled with one donor and one acceptor fluorophore at the N91 position on opposite arms. Samples were preincubated with ATP (left), AMPPNP (middle), and ADP (right). Upper panels: Grp94 adopts discrete conformations with characteristic low and high FRET efficiencies. Solid lines show a double Gaussian fit for ATP and AMPPNP conditions and a single Gaussian fit for ADP conditions. The average and standard deviation of the Gaussian peaks are reported above their distributions. Lower panels: Fluorescence and calculated FRET efficiency traces, for example, individual molecules under each of the three nucleotide conditions. Donor fluorescence (green lines) and acceptor fluorescence (orange lines) from donor excitation are shown above the calculated FRET efficiencies (black lines). Acceptor fluorescence from direct excitation is shown in red lines. Arrows indicate donor (green) and acceptor (red) photobleaching. Experiments were performed with alternating excitation (donor: 650 μW at 532 nm, acceptor: 150 μW at 633 nm). The histogram data come from two fields of view for ATP and one field of view for both ADP and AMPPNP. Buffer conditions 50 mM Hepes (pH 8.0), 150 mM KCl, 0.6 mM $MgCl_2$, 0.6 mM nucleotides, 2 mM BME, and 0.5 mg/ml BSA, at room temperature.

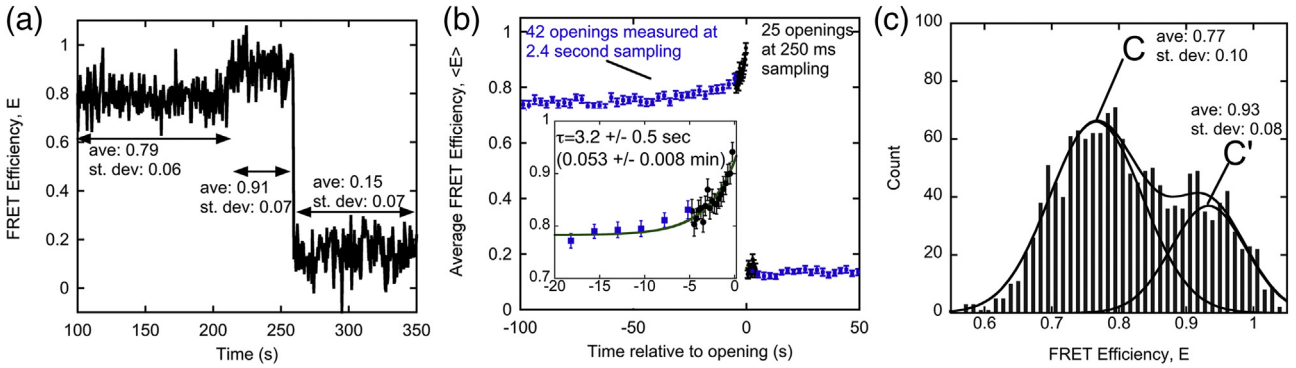

Fig. 3. Grp94 conformational changes under ATP conditions. (A) Example trace under ATP conditions. The average and standard deviation of efficiency values are shown for select regions. (B) Average FRET efficiencies are shown for traces that are aligned at their opening time. Experiments were performed with both alternating excitation (blue squares; donor: 650 μW at 532 nm, acceptor: 150 μW at 633 nm) and continuous excitation (black circles; 2.6 mW at 532 nm). Error bars are the SEM. The inset shows a single exponential fit for the transient FRET increase (baseline fit: 0.78 ± 0.01; intercept fit: 0.92 ± 0.01, where the uncertainty is the standard error). (C) Distribution of FRET efficiency values that were recorded zero to 15 s prior to opening events. The solid lines show a double Gaussian fit with the average and standard deviation reported for both peaks. Buffer conditions same as Fig. 2.

an opening transition and aligned these traces at their opening time. Because the open and closed states of Grp94 have well separated FRET efficiencies, conformational transitions can be reliably identified via thresholding. We identified 42 opening events in records with 2.4-s sampling and 25 opening events in those with continuous donor excitation at 250-ms sampling. When these traces are aligned at their opening time and averaged, a transient increase in FRET is observed prior to opening (Fig. 3B). This increase in FRET follows single exponential kinetics, indicating a higher FRET intermediate with an average lifetime of 3.2 ± 0.5 s. The intercept of the fit in Fig. 3B (<E>0.92 ± 0.01) indicates the average FRET efficiency of this distinct closed conformation.

To confirm that this transient increase in FRET is the result of a single state with a discrete FRET efficiency, we evaluated the distribution of FRET efficiencies within 15 s prior to opening to enrich its population. Two distinct FRET states are evident within this restricted time window (Fig. 3C). One peak resembles the predominant ATP FRET state with an average efficiency of 0.77 (referred to as C), while a higher FRET state is centered at an efficiency of 0.93 (referred to as C′). The center of the C′ peak matches the fit intercept from Fig. 3B, which indicates that the majority of opening events proceed through C′ with minimal opening from the C state. Reversible transitions between C and C′ are sometimes observed in individual traces (Supplemental Fig. 4), indicating that excursions to C′ are not always directly followed by an opening event.

The C′ conformation of Grp94 is favored when the dimer has ATP and ADP on opposite arms

The above results suggest that Grp94 transiently samples an alternative closed conformation (C′) upon ATP hydrolysis. We hypothesized that this alternative conformation is the result of sequential ATP hydrolysis of Grp94, resulting in an intermediate with ADP and ATP on opposite arms. To test this idea, we performed smFRET measurements in mixtures of ADP and ATP, with the expectation that the population of C′ will increase as the population of the mixed ATP/ADP state increases. In contrast to cytosolic Hsp90 homologs, Grp94 favors the binding of ATP over ADP [10]. Therefore, the ATP/ADP heterodimer should be populated at high ADP fractions. Indeed, at a 75% fraction ADP the C′ state is evident in the efficiency distribution (Fig. 4A). The entire efficiency distribution is well fit by three Gaussian-distributed FRET states. The center of the highest FRET distribution (<E>=0.93) matches the center of C′ distribution from Fig. 3C.

To evaluate the robustness of the above results, we performed a series of measurements with variable fractions of ADP (25%, 50%, 75%, 85%). All the resulting FRET efficiency distributions can be fit with three Gaussian-distributed states (Supplemental Fig. 5), yielding consistent values for the average FRET efficiency of the C, C′, and open (O) states (Fig. 4B). We conclude that O, C, and C′ are discrete states of Grp94 with invariant conformations over a wide range of nucleotide conditions.

Grp94 can reversibly transition between C and C′

Collectively, Figs. 3 and 4 indicate that the C′ state of Grp94 is an ATP/ADP intermediate that is populated just prior to opening. The transient lifetime of C′ could result from either rapid hydrolysis of the second ATP, or rapid opening from C′ without a second hydrolysis event. To distinguish between these possibilities, we performed smFRET measurements on a Grp94 heterodimer in which one arm is mutated (E103A) to become catalytically inactive [3]. The first scenario predicts that the wt/E103A heterodimer will have an extended C′ lifetime by suppressing hydrolysis of the second ATP. In contrast, the second scenario predicts that the wt/E103A heterodimer should not extend the C′ lifetime.

A comparison of Fig. 5A to Fig. 2 shows that under ATP conditions the wt/E103A Grp94 heterodimer has a greater population of C and C′ than wt/wt Grp94. Gaussian fitting shows similar FRET efficiencies for C and C′ as is observed for wt/wt Grp94 (inset, Fig. 5A). Similar to the analysis in Fig. 3B, we identified opening transitions by thresholding to evaluate the C′ lifetime. Figure 5B shows average efficiencies of wt/E103A traces that are aligned at their opening time. The C′ lifetime of wt/E103A is longer (8.0 ± 1.4 s) than the C′ lifetime of wt/wt Grp94 (3.2 ± 0.5 s). This comparison suggests that the C′ state of wt/wt Grp94 is hydrolytically active and that its more rapid opening via C′ (relative to the heterodimer) is due to the more rapid transition from an ATP/ADP state to an ADP/ADP state. An important caveat in interpreting the C′ lifetime in Fig. 5B is that the transitions between C and C′ are reversible, as discussed next.

Strikingly, individual traces of the Grp94 wt/E103A heterodimer sometimes show prolonged periods of conformational cycling between C and C′ (Fig. 5C). The transitions between C and C′ have anti-correlated changes in donor and acceptor fluorescence and constant fluorescence of the acceptor dye upon direct excitation (Supplemental Fig. 6). The reversible transitions between C and C′ are equally evident in continuous excitation measurements taken at a higher sampling rate (Supplemental Fig. 7).

We used the ebFRET software [15] to objectively identify transitions between C and C′. This analysis was performed on all 282 traces measured with alternating excitation for the wt/E103A heterodimer.

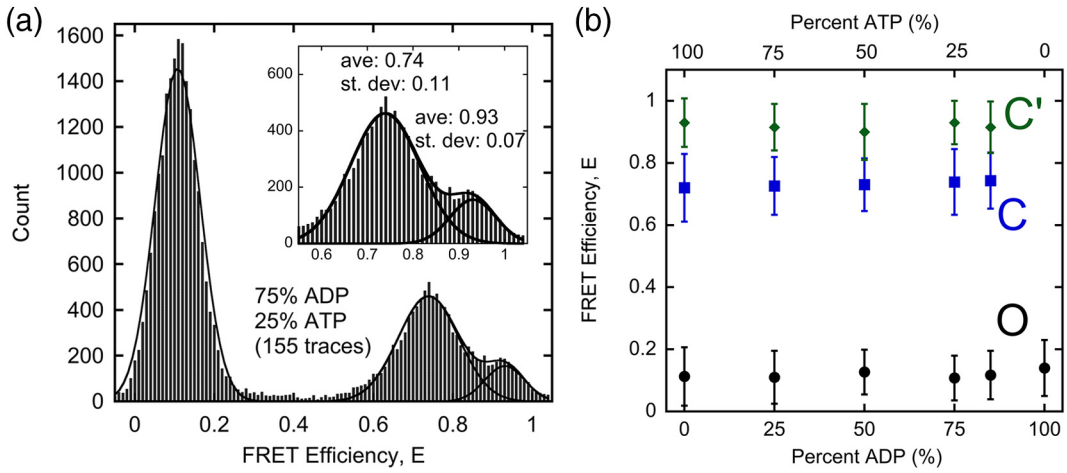

Fig. 4. The C′ conformation of Grp94 is stabilized under mixed nucleotide conditions. (A) At 75% ADP, both the C and C′ FRET states are evident. The solid lines show a triple Gaussian fit. Inset shows the average and standard deviation for the C and C′ efficiency distributions. The histogram data come from one field of view measured with continuous donor excitation (2.6 mW at 532 nm). (B) Summary of Grp94 FRET states under different nucleotide conditions. The average FRET efficiency for different Grp94 conformations is determined from Gaussian fits (100% ATP is from Fig. 3C, 100% ADP is from Fig. 2, the mixed nucleotide conditions are from Supplemental Fig. 5). Errors bars are the peak standard deviations from the Gaussian fits. Buffer conditions same as Fig. 2.

The blue dots in Fig. 5C show an example of the ebFRET-identified states following the visually evident transitions between C and C′. Analyzing all 282 traces by ebFRET yields FRET efficiencies and transition rates for different Grp94 conformational states. The C and C′ states identified by ebFRET (C state: $\langle E \rangle = 0.75 \pm 0.07$; C′ state: $\langle E \rangle = 0.95 \pm 0.04$, mean ± s.d.) are similar to the FRET states identified by Gaussian fitting (Fig. 4B). The open state identified by ebFRET has a higher average FRET and wider distribution ($\langle E \rangle = 0.29 \pm 0.34$) than determined by Gaussian fitting, due to a contribution from a population of mid-range FRET (efficiencies between 0.3 and 0.5 in Fig. 5A). The origin of this additional population of mid-range FRET efficiencies is not known.

The microscopic rate constants determined by ebFRET provide an internal check on the observed opening rate in Fig. 5B, which is the sum of the microscopic rate constants leaving C′. Specifically, the observed rate from aligning wt/E103A traces at their opening time ($1/\tau = 7.5 \pm 1.3$ min^{-1}, Fig. 5B) is within error of the expected observed opening rate from the ebFRET analysis (6.4 ± 0.3 min^{-1}, Fig. 5C), recalling that the observed rate of C′ → O is the sum of the $k_{C'\to O}$ and $k_{C'\to C}$ rate constants. Using similar reasoning $k_{C'\to O}$ for wt/wt can be calculated to be 13.6 ± 2.6 min^{-1} (i.e., the difference between the observed C′ → O rate for wt/wt in Fig. 3B $1/\tau = 18.6 \pm 2.6$ min^{-1}, and $k_{C'\to C}$ from Fig. 5C, 5.0 ± 0.2 min^{-1}).

Figure 6 shows a kinetic model of the Grp94 conformational cycle that integrates smFRET data for both wt/wt and wt/E103A Grp94 (details in Methods). The open-to-closed transition and first hydrolysis step are much slower than the conformational transitions between C and C′ as well as the second hydrolysis step and subsequent opening. The E103A substitution confers striking changes to the smFRET behavior of the wt/E103A Grp94 heterodimer because E103A slows $k_{C'\to O}$ by an order of magnitude, thus enabling more reversible transitions between C and C′ to be observed. As a check on the behavior of this kinetic model, we performed numerical simulations. The model reproduces the experimental behavior of traces aligned at their opening time for both wt/wt and wt/E103A constructs (Supplemental Fig. 8A). The model also predicts a bulk closure rate with ATP that is similar to what is experimentally observed (Supplemental Fig. 8B).

For wt/wt, the model predicts steady-state populations of O (47%), C (53%), and C′ ($\ll$1%) that are comparable to the measured smFRET populations (Supplemental Fig. 5E). However, for wt/E103A, the predicted populations of O (33%), C (65%), and C′ (2%) show differences with the measured populations from Fig. 5A: O (15%), C (69%), and C′ (16%). This discrepancy may be due to the E103A substitution influencing other rate constants in addition to $k_{C'\to O}$.

Discussion

Here we develop a FRET pair that is optimized for Grp94 (Fig. 1A) and discover that this Hsp90 paralog builds up a substantial population of the closed state

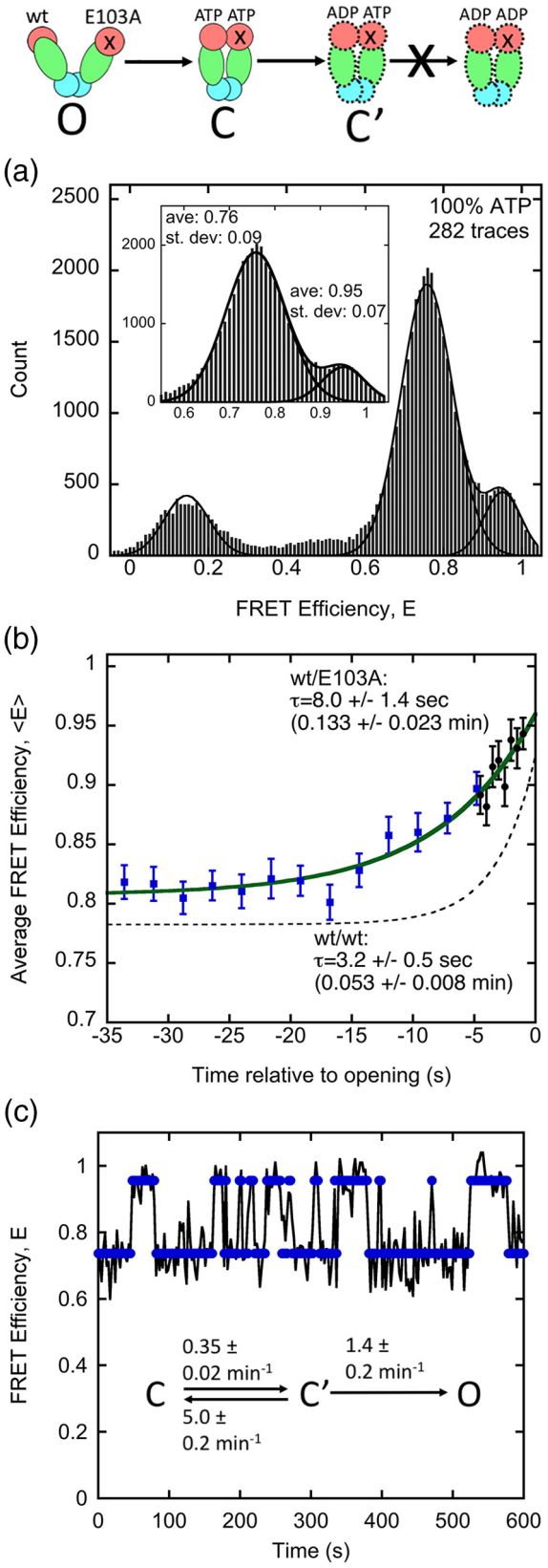

under ATP turnover conditions (Fig. 1B). A natural consequence of populating the closed state under ATP conditions is that the structural changes associated with ATP hydrolysis within the closed state can studied in detail. It was recently shown that cytoplasmic Hsp90 remains functional as a folding chaperone when the N-terminal domains are locked together via the addition of a coiled-coil sequence [8]. This puzzling observation can be understood in light of the results here, according to a mechanism in which ATP-driven conformational changes within the closed state provide the chaperone's essential biological function.

The open and closed states of Grp94 have highly dispersed smFRET efficiency distributions (Fig. 2). Under AMPPNP conditions, Grp94 adopts a high FRET state centered at $E = 0.75$. We ascribe this state to be the symmetric closed conformation on the basis of SAXS analysis (Supplemental Fig. 9). Under ATP conditions, Grp94 undergoes conformational transitions between open and closed states and also adopts an alternative distinct closed conformation, C′, that is transiently sampled from the C state (Fig. 3). This conformational intermediate is populated under mixed nucleotide conditions (Fig. 4) and when ATP hydrolysis is blocked on one arm (Fig. 5). Indeed, blocking the second hydrolysis step allows the wt/E103A heterodimer to more readily undergo cycling between C and C′ before opening (Fig. 5C). Collectively, our results enable the construction of a kinetic model of the Grp94 ATP conformation cycle (Fig. 6). This model shows that sequential ATP hydrolysis steps allow Grp94 to access closed states with very different dynamic properties. In the ATP/ATP state, Grp94 stays within the C conformation, whereas the first hydrolysis event causes Grp94 to enter into a dynamic ATP/ADP state that is capable

Fig. 5. Grp94 conformational cycling between the C and C′ conformations. (A) FRET efficiency histogram for a Grp94 heterodimer (wt/E103A) with only one hydrolytically active arm. The solid lines show a triple Gaussian fit. The histogram data come from one field of view with alternating excitation (donor: 650 μW at 532 nm, acceptor: 150 μW at 633 nm). (B) Average FRET efficiencies for wt/E103A traces that are aligned at their opening time. Experiments were performed with both alternating excitation (blue squares; 2.4-s sampling) and continuous excitation (black circles; 500-ms sampling). Error bars are the SEM. The solid line shows a single exponential fit (baseline fit: 0.81 ± 0.01; intercept fit: 0.96 ± 0.01, where the uncertainty is the standard error). The dashed line shows the fit for wt/wt from Fig. 3B. (C) Example trace showing wt/E103A Grp94 cycling between C and C′. The blue circles show FRET efficiency states assigned by the ebFRET program. Rate constants and uncertainties are the ebFRET output from analyzing all 282 traces. Buffer conditions same as Fig. 2.

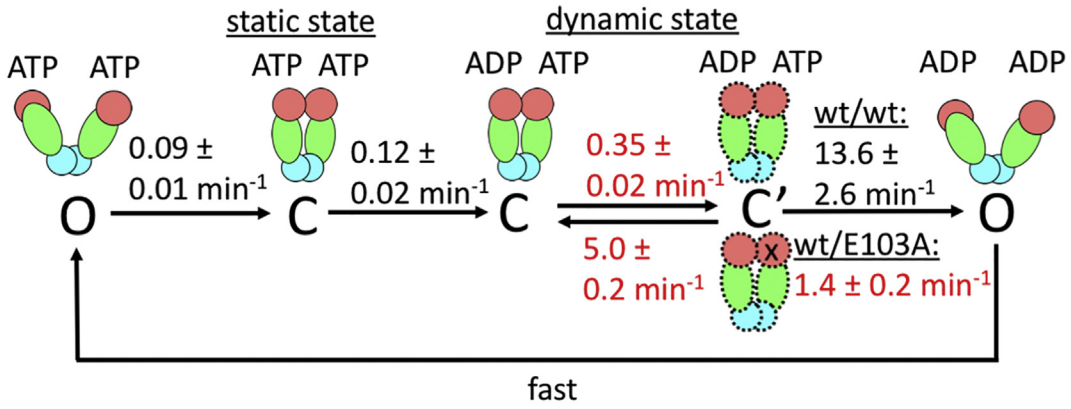

Fig. 6. Kinetic model of Grp94 conformational cycle. Rate constants in black were determined from analysis of wt/wt homodimers (using data from Figs. 2 and 3), and rate constants in red were determined from analysis of wt/E103A heterodimers (using data from Fig. 5).

of cycling between C and C′. The second hydrolysis event leads to an ADP/ADP state that rapidly opens.

Previous studies have provided intimations of closed-state behavior for other Hsp90 paralogs. Work with Trap1 has suggested that sequential ATP hydrolysis results in a conformational change at a client binding site at the MD/CTD interface [12], but it is unclear whether the C′ conformation of Grp94 is a Trap1-like asymmetric closed conformation. An alternative candidate for the C′ conformation is a "coiled-coil" state proposed for Trap1 based on a structure of the dimerized N-terminal domain [16]. Our smFRET data cannot determine whether the C to C′ transition represents a global or a local conformational change.

Extensive FRET analysis has also been performed on yeast Hsp82 both in single-molecule and bulk formats [9,14,17–23]. While the wild-type Hsp82 does not substantially populate the closed conformation under ATP turnover conditions [9,24], kinetic analysis of bulk and single molecule has suggested the presence of two distinct closed conformations [9,17,24]. More work is needed to determine whether the closed-state behavior of Grp94 is applicable to other Hsp90 paralogs.

Methods

Grp94 purification is similar to previously described methods [25]. Purified Grp94 was fluorescently labeled in 25 mM Tris (pH 7.5), 150 mM KCl, 2 mM $MgCl_2$, and 1 mM TCEP for 3 h at room temperature. Grp94 was labeled at a monomer concentration of 25–30 μM with a 5-fold excess of dye (Alexa Fluor 555 C_2 maleimide or Alexa Fluor 647 C_2 maleimide; Thermo Fisher Scientific). The Förster distance for Alexa Fluor 555 (donor) and Alexa Fluor 647 (acceptor) is reported to be 51 Å (Thermo Fisher). After labeling, a 4-fold excess of BME over dye was added to quench the reaction. Labeled Grp94 was separated from free dye via gel filtration. The fluorophore labeling efficiencies for all proteins, 70%–80%, were determined by absorption measurements.

Bulk FRET was measured with a FluoroMax-4 spectrofluorometer (Horiba Scientific). FRET experiments were started by first mixing 125 nM donor-labeled protein and 125 nM acceptor-labeled protein in 25 mM Hepes (pH 8.0), 150 mM KCl, 0.6 mM $MgCl_2$, 2 mM BME, and 0.5 mg/ml BSA at 30 °C for 2 h to form heterodimers. Closure kinetics were initiated with 600 μM nucleotide. Excitation was set at 532 nm, and emission was measured at 565 nm for the donor and 670 nm for the acceptor with slit widths of 1.5 and 4.5 nm for donor and acceptor, respectively. Bulk FRET efficiency was calculated as acceptor/(donor + acceptor).

smFRET

A SNAP tag was cloned at the Grp94 C-terminus, which enabled selective biotinylation via a benzylguanine derivative. The addition of the biotinylated SNAP tag does not significantly change Grp94 closure and reopening properties in bulk FRET experiments (Supplemental Fig. 10). The acceptor-labeled SNAP-Grp94 formed heterodimers with donor-labeled Grp94 under the same conditions as bulk FRET except using 50 mM Hepes buffer. Heterodimers (wt/E103A) of donor-labeled E103A were formed with the acceptor-labeled SNAP–biotin-tagged wt construct. FRET analysis was only performed on spots with a single donor and a single acceptor fluorophore.

Closure was initiated with 600 μM nucleotide, AMPPNP samples were preincubated for at least 3 h at 40 °C, and ATP samples were preincubated for at least 30 min at 30 °C. Different preincubation

times were used for ATP and AMPPNP because Grp94 reaches equilibrium more quickly with ATP *versus* AMPPNP (Fig. 1). The samples were then equilibrated to room temperature for smFRET measurements. Glass slides and coverslips were prepared as previously described [26]. A control in which the slide was pretreated with an excess of free biotin prior to adding Grp94 yielded minimal spots, which shows that the attachment of Grp94 to the slide is via the biotin/streptavidin linkage (Supplemental Fig. 2). Before applying the protein onto the slide, the sample was diluted to 625 pM with an oxygen scavenging system (0.4% glucose, 1.5 units/μl catalase, 0.04 units/μl glucose oxidase) and triplet-state quencher cocktail (2 mM propyl gallate, 4 mM 4-nitrobenzyl alcohol, 4 mM TROLOX). The quencher cocktail increased Grp94 bulk FRET closure rates by a factor of two.

Single-molecule TIRF imaging of Grp94 molecules was performed on a custom microscope as previously described [27]. The acceptor/donor fields collect emission fluorescence from wavelengths greater/less than approximately 635 nm. Grp94 smFRET measurements were performed with two methods of sampling. The slower sampling method (2.4 s between successive measurements) included alternating acceptor and donor excitation, to verify that neither dye photobleached. For alternating excitation experiments, donor and acceptor fluorescences were each measured for 1 s, with the remaining time used for opening and closing shutters on the lasers. For continuous donor excitation at higher sampling rates (either 250 or 500 ms/measurement), a short acceptor excitation was applied afterward to verify which acceptor dyes retained fluorescence. In both cases, FRET analysis was performed on all traces with a donor photobleach event, after which the background fluorescence was subtracted for both the donor and acceptor. FRET efficiency values were only calculated for time points where when both the donor and acceptor fluorophores were not photobleached. Given our time resolution of 250 ms, the open and closed states could represent a time-average of conformations that interconvert much faster than 250 ms.

The smFRET efficiency was calculated as acceptor/(γ*donor + acceptor), where the γ value (1.75) was determined empirically as the value in which the total donor and acceptor fluorescence remains constant. Donor fluorescence data shown in figures are scaled by the gamma factor. Data analysis was performed on custom software implemented in Matlab, which is available online (https://github.com/gelles-brandeis/CoSMoS_Analysis) [27]. Opening transitions were identified by thresholding at $E = 0.5$. We identified 42 opening events in 260 traces measured with alternating excitation, while 25 opening events were observed in 372 traces measured with continuous excitation at 250-ms sampling. Fewer opening transitions were observed under continuous excitation conditions due to more rapid photobleaching.

The microscopic rate constants in Fig. 6 were determined from analysis of wt/wt Grp94 under ATP conditions (data in Fig. 2) and wt/E103A Grp94 under ATP conditions (data in Fig. 5A). The $k_{C\rightarrow C'}$ and $k_{C'\rightarrow C}$ rate constants were determined from the wt/E103A Grp94 data by the ebFRET program [15]. ebFRET was run with three states and a photobleaching correction state, which is an artificial FRET state appended at the end of the trace where photobleaching is experimentally observed. The $k_{O\rightarrow C}$ rate constant was determined from ebFRET analysis of wt/wt Grp94 measured with alternating excitation. Here ebFRET was run with two states and the photobleaching correction. The total dwell time for the wt/wt closed state was also determined by ebFRET, which was then used to calculate the rate associated with the first ATP hydrolysis step in Fig. 6. The model does not include C → O transitions because Fig. 3B indicates that the majority of opening transitions occur via C′ → O. Specifically, the fit intercept in Fig. 3B (<E>=0.92) represents the average FRET efficiency at the opening time, and this value closely matches the C′ peak efficiency from Fig. 3C (<E>=0.93). The $k_{C'\rightarrow O}$ rate for wt/E103A was determined by ebFRET analysis. The $k_{C'\rightarrow O}$ rate constant for wt/wt was determined by the observed reopening rate in Fig. 3B and $k_{C'\rightarrow C}$, as described in Results. The $k_{C'\rightarrow C}$ rate constant is assumed to be the same for wt/wt and wt/E103A because the C′ → C transition does not involve an ATP hydrolysis step. Nucleotide binding and release in the open state was treated as much faster than closure and therefore not a kinetically relevant step, consistent with previous measurements of nucleotide binding kinetics [28].

Numerical simulations of the model in Fig. 6 were performed in Python using Gillespie sampling. The smFRET data predicts a bulk closure rate that is similar to the experimentally measured bulk closure rate (Supplemental Fig. 8), which indicates that the behavior of Grp94 is not significantly perturbed by the attachment to the slide in smFRET experiments.

ATPase activity assay

Enzyme-linked ATPase activity measurements were performed on a temperature-controlled plate reader (BioTek). ATP hydrolysis rates were calculated by the consumption of NADH as measured by absorption at 340 nm. Background measurements without chaperone protein were measured prior to adding the chaperone to the plate. After adding the chaperone, a 5-min shaking step ensures complete mixing.

Acknowledgments

We thank Thorsten Hugel for providing helpful feedback on the results. Research for this project was supported by NIH R01 GM115356 (T.O.S.) and R01 GM121384 and R01 GM81648 (J.G.). SAXS measurements were conducted at the Advanced Light Source.

Appendix A. Supplementary data

Supplementary data to this article can be found online at https://doi.org/10.1016/j.jmb.2019.06.004.

Received 19 February 2019;
Received in revised form 4 June 2019;
Available online 14 June 2019

Abbreviations used:
MD, middle domain; CTD, C-terminal domain; SAXS, small-angle x-ray scattering; smFRET, single-molecule FRET.

References

[1] W.M. Obermann, H. Sondermann, A.A. Russo, N.P. Pavletich, F.U. Hartl, In vivo function of Hsp90 is dependent on ATP binding and ATP hydrolysis, J. Cell Biol. 143 (1998) 901–910.
[2] B. Panaretou, C. Prodromou, S.M. Roe, R. O'Brien, J.E. Ladbury, P.W. Piper, L.H. Pearl, ATP binding and hydrolysis are essential to the function of the Hsp90 molecular chaperone in vivo, EMBO J. 17 (1998) 4829–4836.
[3] O. Ostrovsky, C.A. Makarewich, E.L. Snapp, Y. Argon, An essential role for ATP binding and hydrolysis in the chaperone activity of GRP94 in cells, Proc. Natl. Acad. Sci. U. S. A. 106 (2009) 11600–11605.
[4] M.M. Ali, S.M. Roe, C.K. Vaughan, P. Meyer, B. Panaretou, P.W. Piper, C. Prodromou, L.H. Pearl, Crystal structure of an Hsp90–nucleotide–p23/Sba1 closed chaperone complex, Nature 440 (2006) 1013–1017.
[5] K.A. Verba, R.Y. Wang, A. Arakawa, Y. Liu, M. Shirouzu, S. Yokoyama, D.A. Agard, Atomic structure of Hsp90–Cdc37–Cdk4 reveals that Hsp90 traps and stabilizes an unfolded kinase, Science 352 (2016) 1542–1547.
[6] J.D. Huck, N.L. Que, F. Hong, Z. Li, D.T. Gewirth, Structural and functional analysis of GRP94 in the closed state reveals an essential role for the pre-N domain and a potential client-binding site, Cell Rep. 20 (2017) 2800–2809.
[7] L.A. Lavery, J.R. Partridge, T.A. Ramelot, D. Elnatan, M.A. Kennedy, D.A. Agard, Structural asymmetry in the closed state of mitochondrial Hsp90 (TRAP1) supports a two-step ATP hydrolysis mechanism, Mol. Cell 53 (2014) 330–343.
[8] L. Pullen, D.N. Bolon, Enforced N-domain proximity stimulates Hsp90 ATPase activity and is compatible with function in vivo, J. Biol. Chem. 286 (2011) 11091–11098.
[9] M. Hessling, K. Richter, J. Buchner, Dissection of the ATP-induced conformational cycle of the molecular chaperone Hsp90, Nat. Struct. Mol. Biol. 16 (2009) 287–293.
[10] J.C. Halpin, T.O. Street, Hsp90 sensitivity to ADP reveals hidden regulation mechanisms, J. Mol. Biol. 429 (2017) 2918–2930.
[11] T.O. Street, L.A. Lavery, D.A. Agard, Substrate binding drives large-scale conformational changes in the Hsp90 molecular chaperone, Mol. Cell 42 (2011) 96–105.
[12] D. Elnatan, M. Betegon, Y. Liu, T. Ramelot, M.A. Kennedy, D. A. Agard, Symmetry broken and rebroken during the ATP hydrolysis cycle of the mitochondrial Hsp90 TRAP1, Elife 6 (2017).
[13] J.R. Partridge, L.A. Lavery, D. Elnatan, N. Naber, R. Cooke, D.A. Agard, A novel N-terminal extension in mitochondrial TRAP1 serves as a thermal regulator of chaperone activity, Elife 3 (2014).
[14] C. Ratzke, F. Berkemeier, T. Hugel, Heat shock protein 90's mechanochemical cycle is dominated by thermal fluctuations, Proc. Natl. Acad. Sci. U. S. A. 109 (2012) 161–166.
[15] J.W. van de Meent, J.E. Bronson, C.H. Wiggins, R.L. Gonzalez Jr., Empirical Bayes methods enable advanced population-level analyses of single-molecule FRET experiments, Biophys. J. 106 (2014) 1327–1337.
[16] N. Sung, J. Lee, J.-H. Kim, C. Chang, A. Joachimiak, S. Lee, F.T.F. Tsai, Mitochondrial Hsp90 is a ligand-activated molecular chaperone coupling ATP binding to dimer closure through a coiled-coil intermediate, Proc. Natl. Acad. Sci. 113 (2016) 2952–2957.
[17] M. Mickler, M. Hessling, C. Ratzke, J. Buchner, T. Hugel, The large conformational changes of Hsp90 are only weakly coupled to ATP hydrolysis, Nat. Struct. Mol. Biol. 16 (2009) 281–286.
[18] O.R. Lorenz, L. Freiburger, D.A. Rutz, M. Krause, B.K. Zierer, S. Alvira, J. Cuellar, J.M. Valpuesta, T. Madl, M. Sattler, J. Buchner, Modulation of the Hsp90 chaperone cycle by a stringent client protein, Mol. Cell 53 (2014) 941–953.
[19] S. Schmid, M. Gotz, T. Hugel, Single-molecule analysis beyond dwell times: demonstration and assessment in and out of equilibrium, Biophys. J. 111 (2016) 1375–1384.
[20] C. Ratzke, M. Mickler, B. Hellenkamp, J. Buchner, T. Hugel, Dynamics of heat shock protein 90 C-terminal dimerization is an important part of its conformational cycle, Proc. Natl. Acad. Sci. U. S. A. 107 (2010) 16101–16106.
[21] S. Schmid, T. Hugel, Efficient use of single molecule time traces to resolve kinetic rates, models and uncertainties, J. Chem. Phys. 148 (2018), 123312.
[22] B.K. Zierer, M. Weiwad, M. Rubbelke, L. Freiburger, G. Fischer, O.R. Lorenz, M. Sattler, K. Richter, J. Buchner, Artificial accelerators of the molecular chaperone Hsp90 facilitate rate-limiting conformational transitions, Angew Chem Int Ed Engl 53 (2014) 12257–12262.
[23] A. Rehn, E. Moroni, B.K. Zierer, F. Tippel, G. Morra, C. John, K. Richter, G. Colombo, J. Buchner, Allosteric regulation points control the conformational dynamics of the molecular chaperone Hsp90, J. Mol. Biol. 428 (2016) 4559–4571.
[24] B.K. Zierer, M. Rubbelke, F. Tippel, T. Madl, F.H. Schopf, D.A. Rutz, K. Richter, M. Sattler, J. Buchner, Importance of cycle timing for the function of the molecular chaperone Hsp90, Nat. Struct. Mol. Biol. 23 (2016) 1020–1028.

[25] J.C. Halpin, B. Huang, M. Sun, T.O. Street, Crowding activates heat shock protein 90, J. Biol. Chem. 291 (2016) 6447–6455.
[26] L.J. Friedman, J. Chung, J. Gelles, Viewing dynamic assembly of molecular complexes by multi-wavelength single-molecule fluorescence, Biophys. J. 91 (2006) 1023–1031.
[27] L.J. Friedman, J. Gelles, Multi-wavelength single-molecule fluorescence analysis of transcription mechanisms, Methods 86 (2015) 27–36.
[28] S. Frey, A. Leskovar, J. Reinstein, J. Buchner, The ATPase cycle of the endoplasmic chaperone Grp94, J. Biol. Chem. 282 (2007) 35612–35620.